Past and projected weather pattern persistence with associated multi-hazards in the British Isles

8

Short title: Persistence of weather patterns over the British Isles

10

11 Paolo De Luca[1,2,3*], Colin Harpham[4], Robert L. Wilby[1], John K. Hillier[1], Christian L. E. Franzke[5],

12 Gregor C. Leckebusch[6]

13

14 [1]Geography and Environment, School of Social Sciences, Loughborough University, Loughborough, UK

15 [2]Department of Earth Sciences, Uppsala University, Uppsala, Sweden

16 [3]Centre of Natural Hazards and Disaster Science (CNDS), Uppsala, Sweden

17 [4]Climatic Research Unit (CRU), School of Environmental Sciences, University of East Anglia, Norwich, UK

18 [5]Meteorological Institute and Center for Earth System Research and Sustainability (CEN), University of

19 Hamburg, Hamburg, Germany

20 [6]School of Geography Earth and Environmental Sciences, University of Birmingham, Birmingham, UK

21

22 *Corresponding author

23 E-mail: p.deluca@lboro.ac.uk

24

25

26

27

Abstract

Hazards such as heatwaves and floods are often linked to persistent weather patterns. Atmosphere-Ocean General Circulation Models (AOGCMs) are important tools for evaluating projected changes in extreme weather. Here, we demonstrate that 2-day weather pattern persistence is a useful concept for both investigating climate risks from multi-hazard events as well as for assessing AOGCM realism. This study evaluates the ability of a Coupled Model Intercomparison Project Phase 5 (CMIP5) multi-model sub-ensemble of 10 AOGCMs at reproducing seasonal weather pattern persistence and frequencies over the British Isles. Changes in persistence are investigated under two Representative Concentration Pathways (RCP8.5 and RCP4.5) up to 2100. Broadly, the ensemble replicates historical weather type persistence observed in reanalyses (1971-2000). Future persistence and frequency of summer anticyclonic patterns are found to increase, implying heightened risk of drought and heatwaves. On the other hand, the cyclonic weather type decreases in autumn suggesting reduced likelihood of flooding and severe gales. During winter, AOGCMs suggest increased risk of concurrent flood-wind hazards by 2100, however, they also tend to over-estimate such risks when compared to reanalyses. In summer, the strength of the nocturnal Urban Heat Island (UHI) of London is expected to intensify, enhancing the likelihood of combined heatwave-poor air quality events. Further research is needed to explore other multi-hazards in relation to changing weather pattern persistence and how best to communicate such threats to vulnerable communities.

1. Introduction

Persistent weather patterns can translate into hazards such as heatwaves, poor air quality, drought, wildfires and episodes of flooding [1–4], with significant socio-economic losses [5,6]. Examples of such impactful episodes include the 2003 and 2010 European summer heatwaves that led to more than 100,000 deaths, reduced gross primary productivity of crops and, in the latter episode over Russia, about US$15 billion economic losses [7–10]. Similarly, summer 2013 in eastern China, was the hottest ever recorded in that region, with persistent and widespread heatwaves and droughts causing severe socio-economic impacts amounting to 59 billion RMB in losses [11]. Conversely, the extremely wet and stormy 2013/14 winter over the United Kingdom (UK) was characterised by the passage of numerous low-pressure systems causing extensive pluvial, fluvial, coastal and groundwater flooding along with severe gales [12–14].

A growing body of literature is discussing possible dynamical mechanisms linking Arctic Amplification (AA) [15] (the faster warming of the Arctic compared to the global scale) with more persistent weather patterns across the northern hemisphere mid-latitudes [1–4,16,17]. The influence of AA on the polar jet stream is the dynamical mechanism that has attracted most attention from the media, policy makers and scientists. In fact, since AA began to be observed in the late 1980s, the jet stream has assumed a wavier [2–4,18–20] and weaker [3,4,20,21] character, which accounts for more persistent weather patterns, and hence impactful extreme events in the northern mid-latitudes [16,17,22,23]. Meanwhile, analysis of weather type occurrence and persistence in historical and 21st century climate model runs, under different Representative Concentration Pathways (RCPs), is becoming relevant for assessing the dynamical realism of models as well for describing associated weather and climate extremes [24–27]. By focusing on weather type persistence both model realism and phenomena associated with the AA can be examined.

Natural hazards pose a significant socio-economic threat, yet their spatio-temporal co-occurrence (termed herein *multi-hazards*) are not yet fully understood [28,29]. Multi-hazards/risks research has grown considerably over the last decade [30–34], such that the United Nations Sendai Framework for Disaster Risk Reduction (UNISDR) [35] has called for multi-hazard approaches to disaster risk reduction. Examples of multi-hazard studies include interactions between earthquakes and landslides [36], multi-basin flooding and extra-tropical cyclones [37], river and coastal flooding [38], extreme wet and dry hydrological events [39].

Considering natural hazards as physical processes that can interact across both temporal and spatial scales is of interest to decision makers such as governments, local businesses, emergency management services and (re)-insurance companies. Until recently, natural hazards were almost always considered as independent perils. However, since they can compound in various ways (i.e. occur simultaneously, as cascades or cumulatively) over a sufficiently long time-frame [35], their combined socio-economic impacts can exceed what was originally planned for, putting societies and economies under stress [28].

Previous studies have investigated linkages between weather patterns (or large-scale atmospheric circulation) and local extreme events, such as heavy rainfall, storms, floods and heatwaves [27,37,40–46]. The conventional approach to flood analysis at the *single* catchment scale is being extended to frameworks with inter-related hazards, driven by global climate modes, covering *multiple* catchments [41]. Others show that the bias in simulating regional extreme precipitation days by an Atmosphere-Ocean General Circulation Model (AOGCM) is reduced by applying atmospheric circulation indices [43]. Moreover, weather patterns extracted from AOGCMs have also been used to downscale local climate variables, such as temperature, precipitation, radiation and humidity at local scales [27,47,48]. However, AOGCMs vary in their ability to simulate the frequency, seasonality and persistence of weather patterns at regional scales [27,44]. Some studies have linked heavy precipitation events to

atmospheric circulation states, such as the 850hPa geopotential height field or integrated vapour transport (IVT) [42], and found connections between selected weather patterns and multi-basin flooding driven by extra-tropical cyclones (ETCs) [37]. Others have used weather patterns to quantify changes in the strength of the nocturnal Urban Heat Island (UHI) – a phenomenon that may be associated with combined heatwave and air pollution events within cities [40].

Previous evaluations for Europe and the British Isles (BI) show that Coupled Model Intercomparison Project Phase 5 (CMIP5) AOGCMs generally reproduce synoptic-scale weather patterns, calculated using daily sea-level pressure (SLP) fields, but there are recognized biases [49,50]. For example, CMIP5 AOGCMs are not yet able to simulate correctly the number of anticyclonic (A-type) patterns and hence blocking episodes, with the former being underestimated in northern Europe and the BI, but overestimated in southern Europe [49–51]. Other biases are found for cyclonic (C-type) and westerly (W-type) occurrences, with both being overestimated across Europe [49]. These studies also examined future changes in frequency of weather patterns and blocking episodes by comparing historical conditions with RCP8.5, to determine how such changes might affect European temperatures. The A-type is projected to increase significantly over the BI during all seasons except for winter (DJF), the C-type to decrease in all seasons, and the W-type to increase except in summer (JJA) by the end of the century [49]. Overall, blocking episodes are projected to decrease for the BI in DJF and JJA by 2061-2090 (RCP8.5) [51].

We extend these analyses by assessing the ability of a CMIP5 [52] multi-model sub-ensemble (MME) of 10 AOGCMs at reproducing historical seasonal persistence of daily weather patterns, here identified as Lamb Weather Types (LWTs) over the BI [53–56]. We define 2-day persistence as the probability that a given LWT will occur on any two successive days. Climate model simulations of historic weather patterns are compared with those derived from 20CR [57], NCEP [58] reanalyses, and Lamb's

127 catalogue of subjectively defined weather types [53,59]. We investigate how persistence and seasonal

128 frequencies are projected to change within the full 21st century under RCP8.5 and RCP4.5, with

129 persistence assessed for both the MME mean (MMEM) and individual AOGCMs. We also quantify

130 and discuss the implications of future multi-hazards, here identified as nearly concurrent multi-basin

131 flooding and ETCs impacting Great Britain (GB) in winter [37] or combined summer heatwave and

132 poor air quality events over London [40]. Thus, two multi-hazard metrics are applied, along with their

133 evaluation under RCP8.5 and RCP4.5 projections up to 2100: likelihood of (1) multi-basin flooding

134 (*F-Score*) and (2) changing intensity of the nocturnal *Urban Heat Island (UHI)*.

135

136

137 # 2. Methods and Data

138 ## 2.1 Lamb Weather Types (LWTs)

139 Daily atmospheric sea-level pressure (SLP) patterns are categorized using the system of Lamb Weather

140 Types (LWTs) [53] via an objective classification scheme centred over the BI (Fig 1) [54,56]. Choice

141 of the LWTs objective scheme is justified by the fact that this methodology and weather typing

142 classification was originally developed for the BI. LWTs of similar airflow properties are derived from

143 a 5° by 10° latitude-longitude grid array (Fig 1) and computed from daily (12 UTC) SLP values at

144 each grid point. The airflow characteristics are expressed by the following set of equations, where the

145 integers in bold correspond to the grid point reference numbers in Fig 1:

146

147 $\quad W = \frac{1}{2}(\mathbf{12} + \mathbf{13}) - \frac{1}{2}(\mathbf{4} + \mathbf{5})$ $\qquad$ (westerly flow) $\qquad$ (1)

148

149 $\quad S = 1.74\left[\frac{1}{4}(\mathbf{5} + 2.0 \times \mathbf{9} + \mathbf{13}) - \frac{1}{4}(\mathbf{4} + 2.0 \times \mathbf{8} + \mathbf{12})\right]$ $\qquad$ (southerly flow) $\qquad$ (2)

150

151     $F = (S^2 + W^2)^{1/2}$ (resultant flow)   (3)

152

153     $ZW = 1.07 \left[\frac{1}{2}(\mathbf{15} + \mathbf{16}) - \frac{1}{2}(\mathbf{8} + \mathbf{9}) \right] - 0.95 \left[\frac{1}{2}(\mathbf{8} + \mathbf{9}) - \frac{1}{2}(\mathbf{1} + \mathbf{2}) \right]$

154   (westerly shear vorticity)   (4)

155

156     $ZS = 1.52 \left[\begin{array}{c} \frac{1}{4}(\mathbf{6} + 2.0 \times \mathbf{10} + \mathbf{14}) - \frac{1}{4}(\mathbf{5} + 2.0 \times \mathbf{9} + \mathbf{13}) - \frac{1}{4}(\mathbf{4} + 2.0 \times \mathbf{8} + \mathbf{12}) \\ + \frac{1}{4}(\mathbf{3} + 2.0 \times \mathbf{7} + \mathbf{11}) \end{array} \right]$

157   (southerly shear vorticity)   (5)

158

159     $Z = ZW + ZS$ (total shear vorticity)   (6)

160

161 Flow units are derived from the geostrophic approximation (each equivalent to 1.2 knots) and they are,

162 along with the geostrophic vorticity units, expressed as hPa per 10º latitude at 55ºN (100 units are

163 equivalent to $0.55 \times 10^{-4} = 0.46$ times the Coriolis parameter at 55ºN). Three coefficients are used within

164 equations (2, 4 and 5) to account for variations in relative grid spacing at different latitudes with

165 latitude (ψ) here set as 55º [56]: S is multiplied by 1.74, derived from 1/cos (ψ); ZW, 1.07 and 0.95

166 from sin(ψ)/sin(ψ-5°) and sin(ψ)/sin(ψ+5°); ZS, 1.52 from $1/2(\cos(\psi)^2)$.

167

168 The last step for defining LWTs is to apply five rules [53,54,56]:

169

170 i) the flow direction is given by $\tan^{-1}(W/S)$ and is calculated on an eight-point compass with 45º per

171 sector. If W is positive, add 180º. Thus, the W-type occurs between 247.5˚ and 292.5˚;

172

173 ii) Lamb pure directional weather types (e.g. N, S, or E-types) correspond to an essentially straight

174 flow, when |Z| is less than F;

175

176   iii) Lamb's pure cyclonic (C) and anticyclonic (A) types are identified when $|Z|$ is greater than $2F$,

177   respectively with $Z > 0$ and $Z < 0$;

178

179   iv) Lamb's hybrid types (e.g. AE and CSW) are characterised by a flow partially anticyclonic/cyclonic,

180   with $|Z|$ lying between F and $2F$;

181

182   v) the unclassified (U) type is obtained when F and $|Z|$ are less than 6, with the choice of 6 depending

183   on grid spacing.

184

185   The objective classification scheme yields 27 LWTs comprised of two synoptic types (A and C), five

186   purely directional types (W, NW, E, N, and S) , 19 hybrid combinations of synoptic and directional

187   types (e.g. CNW, CSE and AE), and 1 unclassified (U) type [54,56]. For persistence and frequency

188   analyses, we focus on the 7 synoptic and directional LWTs plus the U-type; counts of hybrid types

189   were spread across the main types as per Lamb's original definition [53,60] and common practice

190   within earlier studies [54,55,61,62]. We assess LWT persistence and frequency for summer (June-

191   July-August, JJA), autumn (September-October-November, SON), winter (December-January-

192   February, DJF) and spring (March-April-May, MAM). On the other hand, when calculating indices of

193   future multi-hazards, the hybrid LWTs were not incorporated into the 7 main types as the F-Score and

194   nocturnal UHI indices require these weather patterns to be considered independently.

195
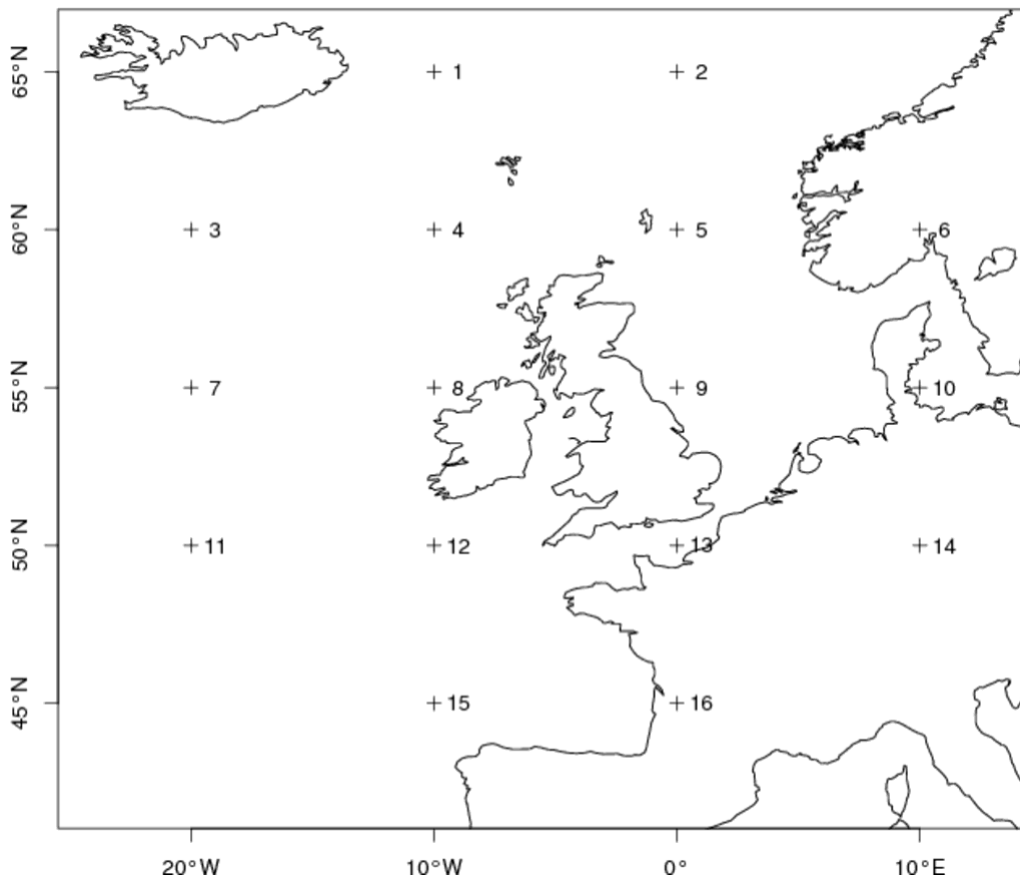
Fig 1. Grid points used to calculate Jenkinson flow and vorticity terms for the British Isles (BI). Numbers refer to those points used in Equations 1 to 5.

2.2 Data

Weather patterns were derived from the SLP produced by each AOGCM in our CMIP5 MME listed in Table 1 [52]. We defined the historical period as the 1980s (1971-2000) whereas the future was divided into three 30-year periods: the 2020s (2011-2040), 2050s (2041-2070) and 2080s (2071-2100). The CMIP5 AOGCMs and MMEM outputs for the historical period was compared with LWTs derived from 20CR [57], NCEP [58] reanalyses and Lamb's subjective catalogue, which ends in 1997 [53,59]. The MMEM was built by first computing the LWTs and relative seasonal persistence and frequencies per each AOGCM then averaging these values within each time period.

2.3 Persistence and trend analyses

Weather pattern persistence is defined here as the conditional probability (p_{jj}) that a given LWT_j on day(t) is followed by the same LWT_j on day($t+1$) [63,64]. This diagnostic was extracted for the 7 main LWTs and the U-type using the diagonal cells of Markov-chain transition matrices. This enabled estimation of historical (1980s) and future (2020s, 2050s and 2080s) seasonal persistence for the MMEM as well as for individual AOGCMs for impactful weather types and seasons, the 20CR, NCEP reanalyses and Lamb's subjective catalogue.

Uncertainty in p_{jj} for the 1980s was calculated by boot-strapping (n=1,000) 30-year seasonal simulations using the *markovchain* package within the R framework [65]. This algorithm stochastically generates *n* series of daily LWTs from the original conditional distributions of the weather patterns in each AOGCM, then recomputes p_{jj} from each series. The resulting $p^{BOOTSTRAP}_{jj}$ is the mean of all p_{jj} across the 1000 series, for each AOGCM. The 95% confidence intervals of $p^{BOOTSTRAP}_{jj}$ are obtained from the cumulative distribution of the 1000 values of p_{jj} for each AOGCM.

Statistical significance of changes in persistence for the AOGCM sub-*ensemble* between the 1980s and future periods (S1 and S2 Tables) was assessed using a Mann-Whitney-Wilcoxon two-tailed test [66] applied to the 10 estimates of $p^{BOOTSTRAP}_{jj}$ for each time period. Changes in p_{jj} between the 1980s and future periods for *individual* AOGCMs were regarded as statistically significant if future persistence of a given LWT and AOGCM fell outside the 95% confidence intervals of the $p^{BOOTSTRAP}_{jj}$ range of that AOGCM for the 1980s (Fig 3 and S2 Fig).

To detect both linear and non-linear annual changes in the total seasonal counts of LWTs MMEM frequencies under RCP8.5 and RCP4.5 scenarios, a trend analysis was performed for the 2006-2100 time period. For illustrative purposes, we only show trends for anticyclonic (A, summer JJA), cyclonic

235   (C, autumn SON) and westerly (W, winter DJF) types as indicators of impactful weather across the BI

236   (Fig 4 and S3 Fig). Results are also presented for the southerly (S, spring MAM) types as this LWT

237   shows most significant changes in seasonal persistence according to the non-parametric Mann-

238   Whitney-Wilcoxon two-tailed test between the 1980s and each of the three future periods (i.e. 2020s,

239   2050s and 2080s). A modified Mann-Kendall test, which takes into account possible autocorrelation

240   within the time series, was applied to both RCP8.5 and RCP4.5 seasonal MMEM LWTs frequencies

241   [67]. The significance of trends, along with their relative Sen's slopes, are shown in S3 Table [68].

242

243   2.4 Indices of winter flood-wind hazards and summer UHI intensity

244   As a measure of concurrent flood-wind hazards we calculated an extended version of the F-Index

245   [37,69], here defined as the F-Score, for each single AOGCM, MMEM, NCEP, 20CR and Lamb's

246   subjective datasets, covering the 1980s, 2020s, 2050s and 2080s, for selected LWTs known to drive

247   these multi-hazard events [37] during winter under both RCP8.5 (Fig 5) and RCP4.5 (S4 Fig). The F-

248   Index is the ratio of observed to expected frequency of floods for a given LWT, where values greater

249   than 1 show higher than expected likelihood. Ten LWTs are known to be associated with historic,

250   multi-basin floods [37], of which eight (C, CS, CSW, CNW, S, SW, W, and NW-types) increase their

251   likelihood and two (N and A-types) reduce likelihood. All other LWTs are weighted zero. The F-Score

252   is then calculated by multiplying the winter DJF frequencies ($freq\_djf_j$) of these LWTs by their

253   F_Index_j (as per Event Set E in [37]) and by summing these values:

254

$$F\_Score_i = \sum_{j=1}^{10} freq\_djf_{j,i} \; x \; F\_Index_{j,i}$$

256   (7)

257

258   where i represents the single AOGCM, NCEP, 20CR and Lamb's subjective datasets within the

259   relative time periods of 1980s, 2020s, 2050s, 2080s and j is the given LWT considered from the 10

260   types mentioned above. The higher the F-Score, the greater the likelihood of concurrent multi-basin

261   flood and wind hazards within winter, over the specified time horizon and RCP scenario.

262

263   As a proxy for combined heatwave and poor air quality hazards occurring during summer, we use

264   observed, simulated and projected nocturnal UHI temperatures in tenths of degree Celsius for London

265   (UK) [40], using the same datasets, time periods and RCPs as per the F-Score (Fig 6 and S5 Fig). The

266   UHI phenomenon is caused by absorption and trapping of heat as well as by changed airflows and

267   sensible heat fluxes within the built environment. The simplest form of UHI metric (used by [40]) is

268   based on the daily temperature difference between an urban and rural reference site (during daylight

269   or night hours). These values may then be stratified by LWT to show the extent to which some weather

270   patterns favour extreme UHI episodes. The UHI metric was derived as follows by: i) multiplying LWT

271   summer JJA frequencies ($freq\_jja_h$) by their respective average UHI intensities taken from [40]

272   (UHI_w_h); ii) summing these values; and iii) dividing the total from step ii) by the total number of

273   days in the period analysed ($days_h$) to give the mean daily UHI intensity:

274

275    $$UHI_i = \sum_{h=1}^{27} \frac{freq\_jja_{h,i} \; x \; UHI\_w_{h,i}}{days_{h,i}}$$

276   (8)

277

278   where i is the same notation as per the F-Score and h refers to the 27 LWTs.

279

280   To assess the statistical significance of changes between the AOGCMs 1980s and future 2020s, 2050s

281   and 2080s periods, for both the F-Score and nocturnal UHI temperatures, we applied a similar approach

12

282   as per persistence. Here, n=1,000 boot-strapped samples of daily LWT series (based on conditional

283   distributions for all seasons combined) were generated for each AOGCM run in the 1980s. Next, the

284   F-Score or UHI were calculated for every series and AOGCM, then averaged and confidence limits

285   established as before. This procedure shows the extent to which estimates for the future indices fall

286   within the 95% confidence range of the boot-strapped estimate for each AOGCM in the 1980s.

287

288   Sample sizes varied depending on the index and AOGCM. For the F-Score, we considered the period

289   1971-2001 to capture January and February of winter 2000/01. Here, models with leap years have a

290   total of 11,323 days, models without leap years 11,315 days and the HadGEM2-ES model (with 360

291   days per year) has 11,160 days. For the UHI, the calendar years 1971-2000 were used as we are

292   interested in summer temperatures, with leap year AOGCMs having 10,958 days, non-leap years

293   models 10,950 days and the HadGEM2-ES 10,800 days.

294

295

296

297

298

299

300

301

302

303

304

305

306

307 **Table 1. CMIP5 multi-model sub-ensemble (MME) used in the analyses.**

Model name	Research institute	Lat-Lon resolution	Ensemble member
HadGEM2-ES	Met Office, United Kingdom	1.25° × 1.875°	r1i1p1
MPI-ESM-LR	Max Planck Institute for Meteorology, Germany	1.9° × 1.9°	r1i1p1
MRI-CGCM3	Meteorological Research Institute, Japan	1.1° × 1.1°	r1i1p1
CNRM-CM5	National Centre for Meteorological Research, France	1.4° × 1.4°	r1i1p1
CanESM2	Canadian Center for Climate Modeling and Analysis, Canada	2.8° × 2.8°	r1i1p1
MIROC5	Model for Interdisciplinary Research on Climate, Japan	1.4° × 1.4°	r1i1p1
CSIRO-Mk3.6.0	Commonwealth Scientific and Industrial Research Organisation, Australia	1.9° × 1.9°	r10i1p1
IPSL-CM5A-LR	Institute Pierre-Simon Laplace, France	1.9° × 3.75°	r1i1p1
CCSM4	National Center for Atmospheric Research, USA	0.94° × 1.25°	r6i1p1
GFDL-CM3	Geophysical Fluid Dynamics Laboratory, USA	2° × 2.5°	r1i1p1

308

309 The columns in Table 1 show the: (1) CMIP5 model name; (2) research institute where the model was
310 developed; (3) resolution as latitude by longitude in degrees; and (4) ensemble member analysed. For all models
311 the historical and RCP8.5 (and RCP4.5) sea-level pressure (SLP) outputs are used to calculate daily LWTs for
312 the BI.

313

314

315

14

3 Results

3.1 Persistence of weather patterns (MME)

The A, C and W patterns are the most frequent weather types affecting the BI. Overall, the MME replicates weather type persistence during the four climatological seasons when compared with 20CR [57] and NCEP [58] reanalyses for the historical period (1980s) (Fig 2). There is less agreement between Lamb's subjectively classified daily weather catalogue and both the MME and reanalyses. A-type persistence is more variable within the MME and on average underestimated in winter, consistent with previous studies [49,50]. There is closer agreement for the A-type in other seasons.

W-type persistence agrees with the reanalyses but is always less than in Lamb's catalogue. C-type persistence is overestimated by the MME in all seasons when compared to reanalyses as reported before [49] for Europe more generally. Such biases in the C-type could be interpreted as exaggerating the likelihood of flooding in the MME compared with reanalyses [69].

Fig 2 shows that the distributions of persistence are asymmetrical (or skewed) around the MME means for many of the weather types and time periods. This characteristic suggests potentially large biases in the estimation of extreme events, if studies rely on only single or a few AOGCMs. Changes in weather type persistence between the ensembles of historical and future periods within RCP8.5 (Fig 2) are weakly significant (p-value<0.1, Mann-Whitney-Wilcoxon two-tailed test) for the C-type in summer and autumn by 2080s; W-type in winter by 2050s; E-type in summer by 2080s and winter for the 2020s and 2050s; N-type in spring by 2050s and 2080s; and S-type in summer by 2080s, autumn in all periods and spring by 2050s and 2080s (S1 Table).

339 Results for RCP4.5 show similar changes in persistence compared to RCP8.5, although they are less

340 substantial (S1 Fig). In particular, the C-type is found to change significantly (p<0.1) only in summer

341 by the 2080s; the E-type in winter by the 2080s; the N-type only in spring by the 2080s; and the S-

342 type in summer by the 2050s and spring also by the 2020s (S2 Table).

343

344
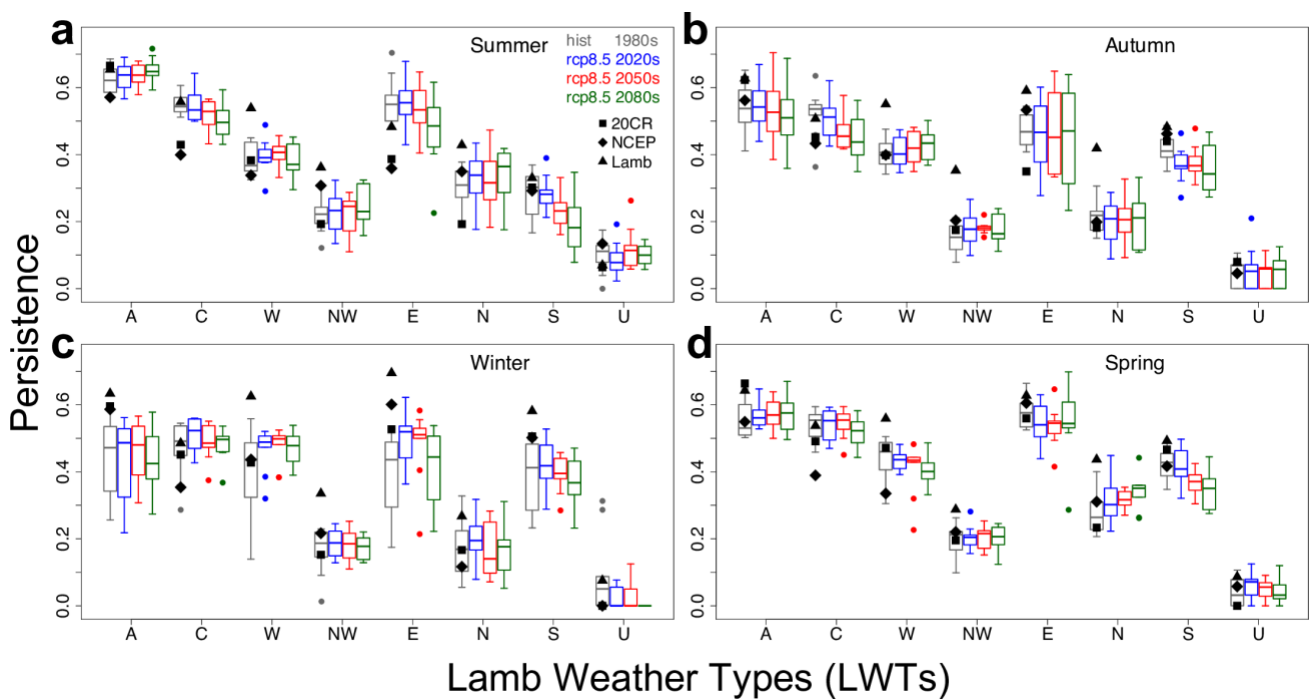
345

346 **Fig 2. Persistence of the seven main LWTs plus unclassified (U) type under RCP8.5.** Persistence is

347 calculated for (a) summer, (b) autumn, (c) winter and (d) spring, for the historical 1980s period (1971-2000)

348 and under RCP8.5 by the 2020s (2011-2040), 2050s (2041-2070) and 2080s (2071-2100). Boxplots show

349 distributions of persistence in each LWT, for the 10-member AOGCM ensemble, compared with 20CR, NCEP

350 and the Lamb's catalogue. Segments show the minimum, 1st quartile, median, 3rd quartile and maximum.

351 Outliers are shown by dots.

352

353

354 ## 3.2 Persistence of weather patterns (by model)

355 Fig 3 shows persistence for the same future periods but for each AOGCM in the MME compared with

356 the reanalyses and Lamb's catalogue, for impactful weather types and seasons. Significance of changes

357   was assessed against the boot-strapped confidence limits for the 1980s. Most model projections under

358   RCP8.5 fall outside the 95% confidence intervals of historical persistence. A-type MMEM persistence

359   increases during summer (Figs 2a and 3a); C-type persistence decreases in all seasons, most markedly

360   in summer and autumn (Figs 2 and 3b); W-type persistence does not change in winter but increases in

361   autumn and decreases in spring (Figs 2b-d and 3c).

362

363   Amongst the other weather types, we note only a decrease in C- and E-types during summer, an

364   increase in N-type in spring, and S-type persistence decreases in all seasons (Figs 2 and 3d). The

365   AOGCMs showing the largest change in A-type persistence during summer are CNRM-CM5, GFDL-

366   CM3 and MIROC5, with a significant increase of 0.061, 0.059 and 0.035 respectively between 1980s

367   and 2080s. For the C-type in autumn, CSIRO-Mk3.6.0, GFDL-CM3 and HadGEM2-ES show a

368   significant decrease in persistence, between 1980s and 2080s, of 0.157, 0.140 and 0.098 respectively.

369   During winter, for the W-type, the AOGCMs showing the largest change, between the same 1980s and

370   2080s periods, are MRI-CGCM3, CanESM2 and CSIRO-Mk3.6.0 with a significant increase in

371   persistence of 0.367, 0.334 and 0.092 respectively.

372

373   Analysis of RCP4.5 output shows similar, though less marked, results when compared to RCP8.5 (S2

374   Fig). Under the lower emission scenario, we find that most AOGCMs project persistence that falls

375   outside the 95% confidence intervals of the 1980s. A-type MMEM persistence in summer is expected

376   to slightly increase, in particular during the 2080s (Figs S1a-S2a), C-type in autumn may decrease

377   (Figs S1b-S2b), W-type during winter is projected to remain stable across the three future periods (Figs

378   S1c-S2c) and S-type persistence in spring decreases by 2100 (Figs S1d-S2d). Other weather types

379   changes in persistence are found for C-type in summer and A-type in autumn which are set to decrease

380   and a marked increase in E-type during winter; the latter are not in agreement with RCP8.5 (S1 Fig).

381
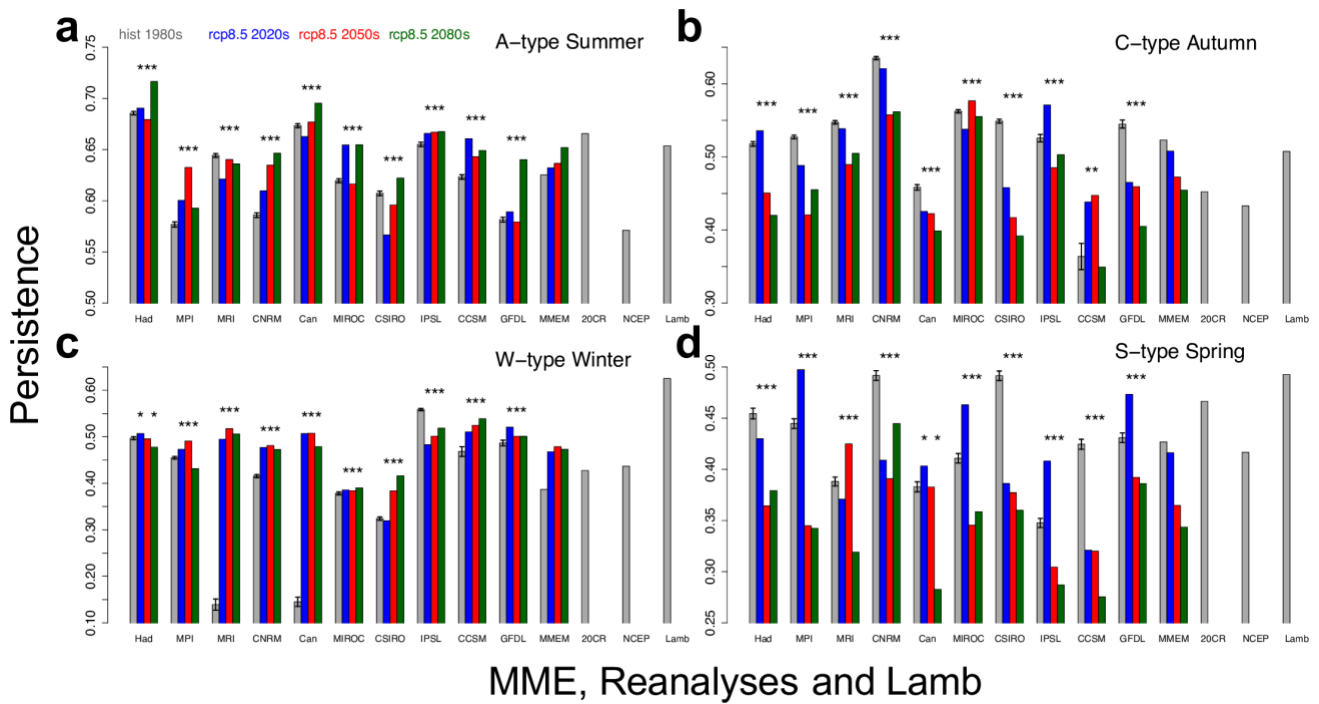
Fig 3. Persistence of selected LWTs and seasons for individual AOGCMs under RCP8.5. (a) A-type (summer), (b) C-type (autumn), (c) W-type (winter) and (d) S-type (spring) in the 1980s compared with the 2020s, 2050s and 2080s under RCP8.5. Persistence is shown for individual AOGCMs alongside the MMEM, 20CR, NCEP and Lamb's catalogue. Asterisks (*) show model runs with persistence outside the 95% confidence intervals of the boot-strapped (n=1,000) estimates for the 1980s, shown here as black T-bars.

3.3 Frequency of weather patterns (MMEM)

Projected frequency trends for selected weather types and seasons under RCP8.5 (2006-2100) are shown in Fig 4. Summer A- and winter W-type frequencies are expected to rise significantly (p<0.01, S3 Table) by 0.8 and 0.2 days per decade respectively over the period 2006-2100. Conversely, C- and S-type frequencies decrease significantly (p<0.01, S3 Table) in autumn and spring respectively. No significant trends are found for C-type frequency during winter. Sen's slopes for the MMEM with their statistical significance are given in S3 Table for each weather type, season and RCP. We also computed the Sen's slopes for A-type in each individual AOGCM during summer (RCP8.5, not shown here) to check whether the increase in A-type was solely due to a few models showing a large increase in this weather type. We found that all models within the MME show a positive increase in A-type frequency,

400   with 7 out of 10 AOGCMs showing significance at the 90% level, with no outliers skewing the

401   MMEM. Among other seasons (not shown), a significant decrease in annual frequencies is observed

402   for the C-type during summer ($p<0.01$) and spring ($p<0.05$), along with a significant ($p<0.01$) increase

403   in A-type during spring, which all reflect the changes in persistence (Fig 2a and 2d).

404

405   Projections of MMEM frequencies for the same LWTs and seasons but under RCP4.5 are shown in

406   S3 Fig and S3 Table. Results for RCP4.5 reflect the scenarios of RCP8.5 although the Sen's slopes are

407   less extreme and statistically significant. The A-type frequency is projected to increase significantly

408   ($p<0.01$, S3a Fig and S3 Table) during summer, C-type in autumn is set to decrease ($p<0.05$, S3b Fig),

409   W-type frequency in winter shows no significant trend (S3c Fig), and the S-type during spring

410   decreases significantly ($p<0.05$, S3d Fig). As per RCP8.5, we also observe (not shown) a significant

411   decrease in C-type frequencies during summer ($p<0.01$) and spring ($p<0.05$) and an increase in the A-

412   type during spring ($p<0.05$), matching the relative changes in persistence (Figs S1a and S1d).

413

414

415
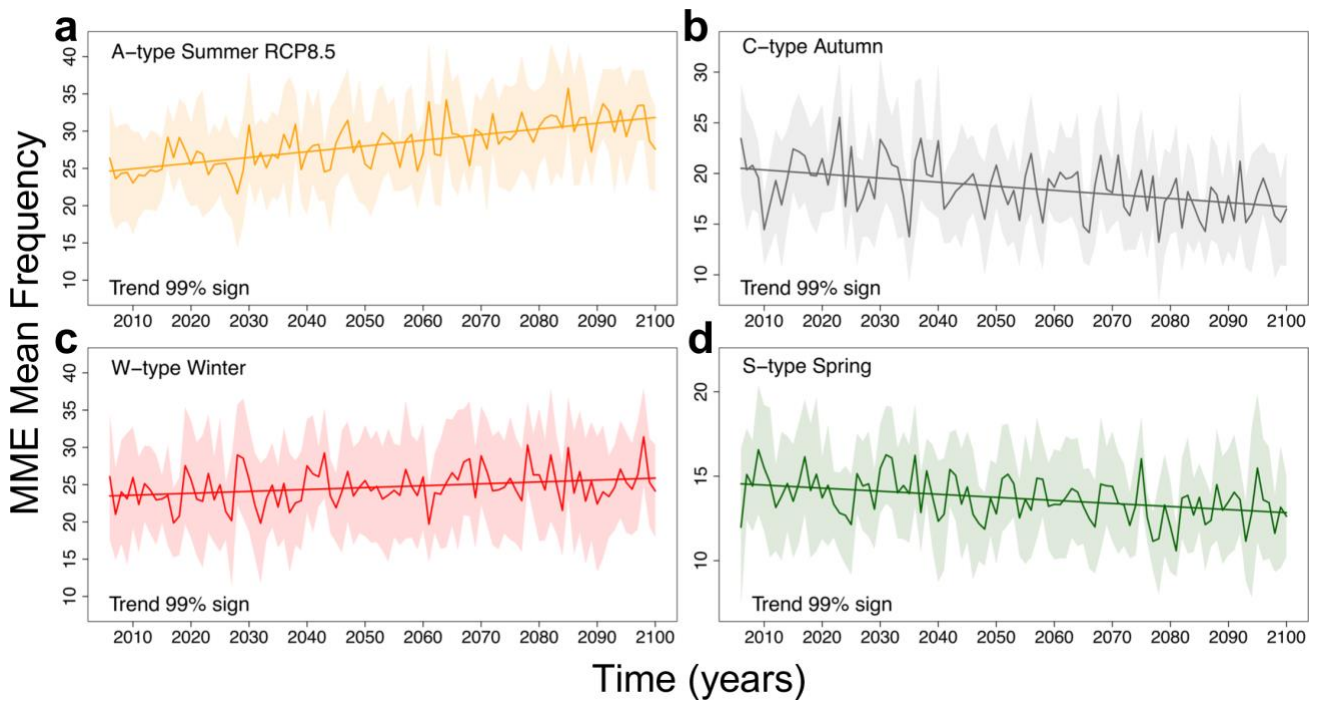
Fig 4. Projected annual frequencies for selected LWTs and seasons under RCP8.5. Frequencies are shown as MMEM for (a) summer anticyclonic A, (b) autumn cyclonic C, (c) winter westerly W and (d) spring southerly S LWTs under RCP8.5 (2006-2100). Trends are statistically significant at the 1% level (p-value<0.01, modified Mann-Kendall test). Shaded areas represent the 95% confidence intervals of the MMEM. The trend lines refer to the Sen's slopes calculated with the modified Mann-Kendall test.
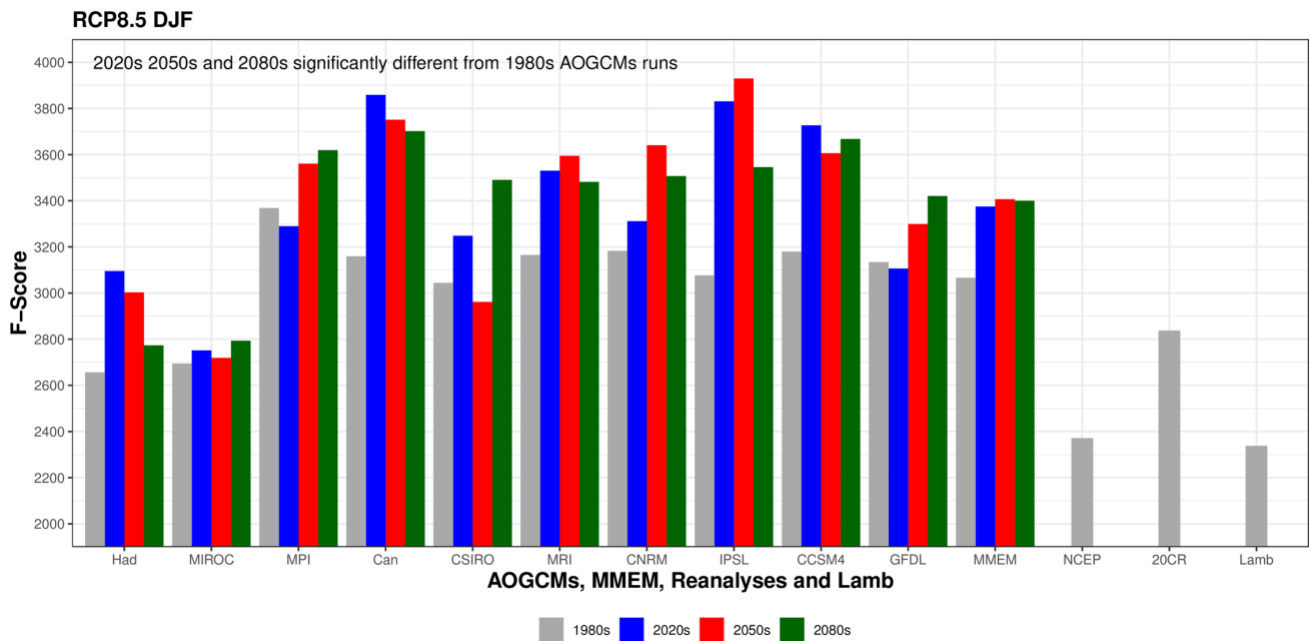
3.4 Application to future multi-hazards

In Fig 5 we extend an earlier analysis [37] based on impactful LWTs found to generate concurrent flood-wind hazards in GB. Thus, the F-Score for each single AOGCM, MMEM, NCEP, 20CR and Lamb's subjective datasets and 1980s, 2020s, 2050s and 2080s time periods are shown for winter DJF weather patterns under RCP8.5. The F-Score is a measure of the severity of future concurrent flood-wind hazards, such that higher values represent more severe impacts compared to lower ones. Here, we show that the baseline risk from multiple flood-wind hazards is overestimated by all but two of the AOGCMs (i.e. HadGEM2-ES and MIROC5) when compared to NCEP, 20CR reanalyses and Lamb's subjective catalogue for the 1980s. Assuming the same bias holds in the future, AOGCMs likely overestimate *absolute* future risk from concurrent flood-wind hazards by 2100. Moreover, in a similar

434   way as per Fig 3, there exists a large variability between the AOGCMs, so F-Score results are mixed

435   with some AOGCMs suggesting increased/decreased risk of flood-wind hazards by the end of the 21st

436   century. It is, therefore, always important to use large ensembles to characterise uncertainty in the

437   projections. Lastly, by looking at the MMEM we conclude that, although overestimated by AOGCMs,

438   future risk from concurrent flood-wind hazards could increase by 2100 compared with the 1980s.

439   Among the AOGCMs, those showing the largest F-Score increase between the 1980s and 2080s are

440   CanESM2, CCSM4 and IPSL-CM5A-LR. Results for RCP4.5 are shown in S4 Fig and they agree with

441   what was found for RCP8.5, with large variability amongst AOGCMs and MMEM F-Score even

442   slightly higher than RCP8.5.

443

444

445

446

447

448

449

450

RCP8.5 DJF

2020s 2050s and 2080s significantly different from 1980s AOGCMs runs

Legend: 1980s, 2020s, 2050s, 2080s

X-axis: AOGCMs, MMEM, Reanalyses and Lamb
Y-axis: F-Score

Fig 5. F-Score for LWTs associated with concurrent flood-wind hazards during winter DJF. The F-Score is shown per each CMIP5 AOGCM, MMEM, NCEP, 20CR and Lamb's subjective catalogue for the 1980s, 2020s, 2050s and 2080s periods. The LWTs used for calculating the F-Score are associated with concurrent multi-basin floods and wind hazards within Great Britain (GB) [37]. The 1980s MME F-Score were estimated from the mean of n=1,000 boot-strapped samples and all the future 2020s, 2050s and 2080s periods are significantly different from these, as the F-Score of the latter fall outside the 95% confidence intervals of the 1980s means. The AOGCMs 1980s confidence intervals bars are not shown for simplicity because they are vanishingly narrow.

Summer nocturnal UHI temperatures in tenths of °C for London (UK), were estimated for RCP8.5, by using UHI values obtained in a previous study [40] (Fig 6). Our results show that AOGCMs replicate nocturnal UHI temperatures, although there is a tendency for underestimation by the majority of AOGCMs except HadGEM2-ES and MIROC5 which show a good agreement when compared to NCEP, 20CR and Lamb's subjective catalogue. We also note that there is less variability within the MME than displayed in Figs 3 and 5. Lastly, almost all the AOGCMs and MMEM show a statistically significant increase in UHI by the end of 2100, that could eventually translate into an increased multi-hazard risk from heatwave and poor air quality events associated with persistent A weather types [40,70–72]. The projected increase in the MMEM UHI between the 1980s and 2080s is 0.15 °C under

471 RCP8.5. The AOGCMs that show the largest increase in nocturnal UHI temperatures between 1980s

472 and 2080s are CanESM2, HadGEM2-ES and CCSM4 with respectively 0.23, 0.22 and 0.22 °C. Results

473 for RCP4.5 agree with the RCP8.5 projections although the changes are less marked (S5 Fig).

474

475

476
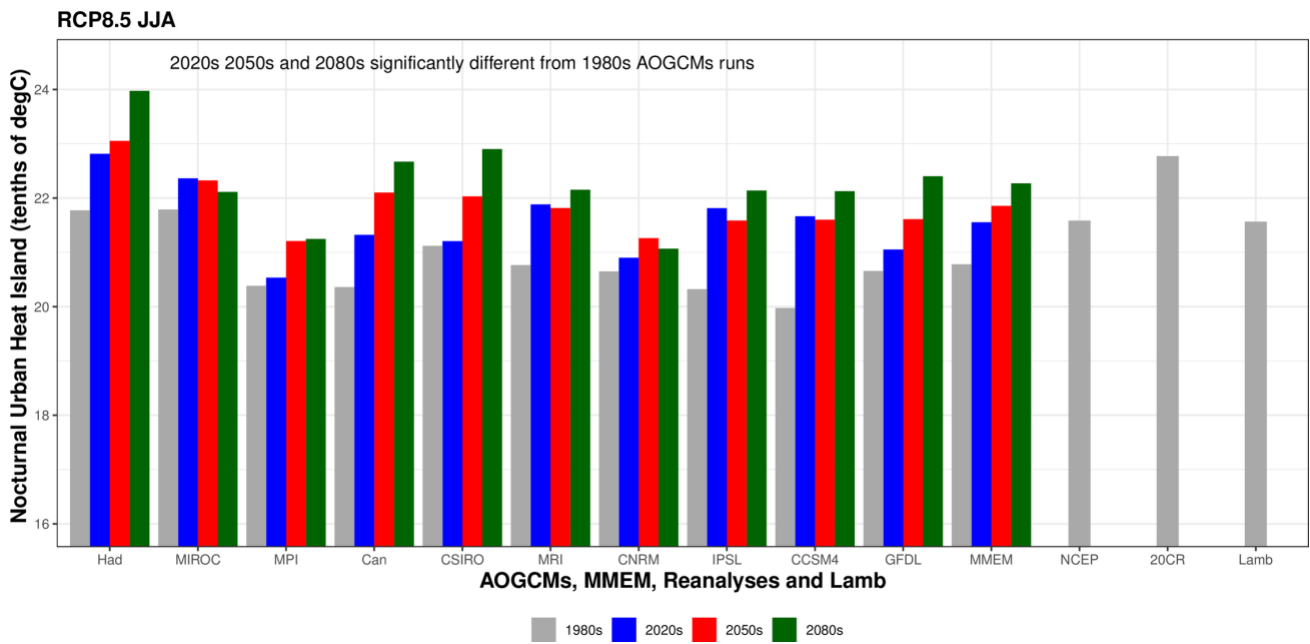
Fig 6. As per Fig 5 but for London's nocturnal UHI in tenths of °C during summer JJA.

478

479

4. Discussion and Conclusions

481 Greater A-type persistence and frequency during summer likely implies more blocking episodes with

482 increased risk of poor air quality, drought and heatwaves [1,5,20]. A growing number of studies

483 propose physical mechanisms that link AA [15] to more persistent weather patterns, which in turn

484 enhance the likelihood of extreme weather events in the northern hemisphere mid-latitudes. The AA

485 affects the polar jet stream by making Rossby waves more meridional (or wavier) and by weakening

486 its flow. A wavier and weaker jet stream in summer favours more persistent extreme weather and it is

487 also thought to extend ridges northward, enhancing such effects [1–3,17,20–22].

23

488

489 Our results support earlier analysis [49], and are consistent with the proposed mechanisms linking

490 *observed* AA with mid-latitude weather extremes. On the other hand, AA is expected to have limited

491 effect on simulated CMIP5 blocking over Eurasia under RCP8.5 in the second half of the 21st century

492 [73]. Other work also shows an overall decrease in CMIP5 blocking events over the BI in winter DJF

493 and summer JJA, during 2061-2090 (RCP8.5) [51]. Our findings for anticyclonic weather appear to

494 contradict this. Although A-type persistence and frequency are not exactly the same as blocking, we

495 would expect the studies to agree as both mechanisms involve high pressure weather patterns. The

496 only common denominator between our findings and the studies on blocking [51,73] seems to be the

497 underestimation of A-type/blocking events by CMIP5 models. Further research is needed to reconcile

498 these apparently contradictory findings. Possible explanations are that results depend on the exact

499 spatial domain and/or suite of AOGCMs analysed in each MME, as well as on the methodology used

500 to define A-type days and blocking events.

501

502 Less persistent C-types in autumn suggests lower likelihood of heavy rainfall, with reduced recharge

503 of soil moisture and aquifers at the start of the hydrological year favouring winter droughts. Fewer

504 cyclonic days may also translate into less frequent severe gales and flooding episodes [69], as in GB

505 extreme multi-basin flooding events are strongly associated with C-type weather over time windows

506 from 1 to 19 days [37]. Conversely, more frequent zonal airflow (W-type) in winter may counteract

507 some loss of precipitation from the C-type, especially across higher elevation regions of the north and

508 west BI where there is strong orographic enhancement [74]. Such changes may be attributed to AA,

509 however, the physical mechanisms linking AA to changes in northern hemisphere mid-latitude

510 circulation currently remains an open question.

511

512 From our analyses it is also possible to infer future changes with respect to multi-hazards [28,30],

513 through the F-Score and nocturnal UHI temperatures. Recent analyses show that in GB nearly

514 concurrent multi-basin flooding and extreme wind events are driven by selected LWTs mainly

515 associated with C- and W-types [37]. These multi-hazard events can generate significant economic

516 losses, hence projections of such events may help in evaluating future risks and in improving resilience.

517 We show that during winter DJF the AOGCMs overestimate the F-Score when compared to NCEP,

518 20CR reanalyses and Lamb's subjective dataset. Even so, by the end of 2100 the MMEM shows a

519 statistically significant increase in the F-Score compared with the 1980s within those same models,

520 suggesting that the risk of concurrent flood-wind impacts may become more severe in a warmer world.

521

522 Nocturnal UHI temperatures in London modelled by AOGCMs agree with NCEP, 20CR and Lamb's

523 subjective datasets, although they are slightly underestimated for the 1980s. Nocturnal UHI severity

524 is expected to increase by 2100 under RCP8.5 (MMEM). Our results confirm an increasing trend of

525 ~0.3 °C in nocturnal UHI in London found in an earlier study over the observational period 1950-2006

526 [40]. Our findings are also in line with the UK Climate Projections Science Report 2009 [75] which

527 suggests that intense UHI events are highly correlated with A-type weather patterns, and that in

528 London, intense UHI summer events are expected to become more severe in the future [76]. However,

529 further analysis of projections of UHI is needed with a larger model ensemble to better account for

530 uncertainty. Our present findings, when coupled with a significant increase in persistence and

531 frequency of A-type weather pattern, suggests a combined increased risk of heatwaves and poor air

532 quality events in London [40,70–72,76] that could negatively impact human health.

533

534 Finally, we have illustrated how changes in the persistence and frequency of weather patterns are

535 useful diagnostics of climate model realism and can translate into regional to local weather and climate

536 risks scenarios, which could be helpful for developing narratives for decision-makers. However,

caution needs to be taken when qualitatively converting synoptic weather pattern changes into local variability because AOGCM skill in reproducing climatic variables at local scales varies significantly and is not always consistent with observations. This is particularly true for precipitation where, for example, pressure fields alone are not able to provide reliable local projections [27].

With the UK Climate Projections 2018 now partly released and planning underway for the third UK Climate Change Risk Assessment, weather pattern analysis could help to both evaluate the new projections and offer ways of explaining changes that are intelligible to a range of user communities. Similar links to persistence could be made in other regions with established weather pattern typologies, such as the *Grosswetterlagen* for Europe [77], hydrologically important weather types in the contiguous United States [78] and Spatial Synoptic Classification for North America [79].

References

[1]   Coumou D, Di Capua G, Vavrus S, Wang L, Wang S. The influence of Arctic amplification on mid-latitude summer circulation. Nat Commun 2018;9:2959. doi:10.1038/s41467-018-05256-8.

[2]   Francis J, Skific N. Evidence linking rapid Arctic warming to mid-latitude weather patterns. Philos Trans R Soc London A Math Phys Eng Sci 2015;373. doi:10.1098/rsta.2014.0170.

[3]   Francis JA, Vavrus SJ. Evidence linking Arctic amplification to extreme weather in mid-latitudes. Geophys Res Lett 2012;39. doi:10.1029/2012GL051000.

[4]   Francis JA, Vavrus SJ. Evidence for a wavier jet stream in response to rapid Arctic warming. Environ Res Lett 2015;10:14005.

[5]   Munich Re. Natural catastrophes 2014: Analyses, assessments, positions. 2015.

[6]   Munich Re. NatCatSERVICE - Natural catastrophes in 2018. 2019.

[7]   Stott PA, Stone DA, Allen MR. Human contribution to the European heatwave of 2003. Nature 2004;432:610–4. doi:10.1038/nature03089.

[8]   Barriopedro D, Fischer EM, Luterbacher J, Trigo RM, García-Herrera R. The Hot Summer of 2010: Redrawing the Temperature Record Map of Europe. Science (80-) 2011;332:220 LP-224. doi:10.1126/science.1201224.

[9]   Bastos A, Gouveia CM, Trigo RM, Running SW. Analysing the spatio-temporal impacts of the 2003 and 2010 extreme heatwaves on plant productivity in Europe. Biogeosciences 2014;11:3421–35. doi:10.5194/bg-11-3421-2014.

[10]   Le Tertre A, Lefranc A, Eilstein D, Declercq C, Medina S, Blanchard M, et al. Impact of the 2003 Heatwave on All-Cause Mortality in 9 French Cities. Epidemiology 2006;17:75–9.

[11]   Sun Y, Zhang X, Zwiers FW, Song L, Wan H, Hu T, et al. Rapid increase in the risk of extreme summer heat in Eastern China. Nat Clim Chang 2014;4:1082.

[12]   Muchan K, Lewis M, Hannaford J, Parry S. The winter storms of 2013/2014 in the UK:

587 hydrological responses and impacts. Weather 2015;70:55–61. doi:10.1002/wea.2469.

588 [13] Kendon M, McCarthy M. The UK's wet and stormy winter of 2013/2014. Weather

589 2015;70:40–7. doi:10.1002/wea.2465.

590 [14] Matthews T, Murphy C, Wilby RL, Harrigan S. Stormiest winter on record for Ireland and

591 UK. Nat Publ Gr 2014;4:738–40. doi:10.1038/nclimate2336.

592 [15] Screen JA, Simmonds I. The central role of diminishing sea ice in recent Arctic temperature

593 amplification. Nature 2010;464:1334.

594 [16] Cohen J, Pfeiffer K, Francis JA. Warm Arctic episodes linked with increased frequency of

595 extreme winter weather in the United States. Nat Commun 2018;9:869. doi:10.1038/s41467-

596 018-02992-9.

597 [17] Cohen J, Screen JA, Furtado JC, Barlow M, Whittleston D, Coumou D, et al. Recent Arctic

598 amplification and extreme mid-latitude weather. Nat Geosci 2014;7:627.

599 [18] Hanna E, Hall RJ, Overland JE. Can Arctic warming influence UK extreme weather? Weather

600 2017;72:346–52. doi:10.1002/wea.2981.

601 [19] Screen JA, Simmonds I. Exploring links between Arctic amplification and mid-latitude

602 weather. Geophys Res Lett 2013;40:959–64. doi:10.1002/grl.50174.

603 [20] Tang Q, Zhang X, Francis JA. Extreme summer weather in northern mid-latitudes linked to a

604 vanishing cryosphere. Nat Clim Chang 2013;4:45.

605 [21] Francis JA, Vavrus SJ, Cohen J. Amplified Arctic warming and mid-latitude weather: new

606 perspectives on emerging connections. Wiley Interdiscip Rev Clim Chang 2017;8:e474.

607 doi:10.1002/wcc.474.

608 [22] Francis JA. Why Are Arctic Linkages to Extreme Weather Still up in the Air? Bull Am

609 Meteorol Soc 2017;98:2551–7. doi:10.1175/BAMS-D-17-0006.1.

610 [23] Di Capua G, Coumou D. Changes in meandering of the Northern Hemisphere circulation.

611 Environ Res Lett 2016;11:94028.

612 [24] Franzke CLE. Persistent regimes and extreme events of the North Atlantic atmospheric

613 circulation. Philos Trans R Soc London A Math Phys Eng Sci 2013;371.

614 doi:10.1098/rsta.2011.0471.

615 [25] Hannachi A, Straus DM, Franzke CLE, Corti S, Woollings T. Low-frequency nonlinearity and

616 regime behavior in the Northern Hemisphere extratropical atmosphere. Rev Geophys

617 2017;55:199–234. doi:10.1002/2015RG000509.

618 [26] Sillmann J, Thorarinsdottir T, Keenlyside N, Schaller N, Alexander L V, Hegerl G, et al.

619 Understanding, modeling and predicting weather and climate extremes: Challenges and

620 opportunities. Weather Clim Extrem 2017;18:65–74.

621 doi:https://doi.org/10.1016/j.wace.2017.10.003.

622 [27] Murawski A, Bürger G, Vorogushyn S, Merz B. Can local climate variability be explained by

623 weather patterns? A multi-station evaluation for the Rhine basin. Hydrol Earth Syst Sci

624 2016;20:4283–306. doi:10.5194/hess-20-4283-2016.

625 [28] Zscheischler J, Westra S, van den Hurk BJJM, Seneviratne SI, Ward PJ, Pitman A, et al.

626 Future climate risk from compound events. Nat Clim Chang 2018;8:469–77.

627 doi:10.1038/s41558-018-0156-3.

628 [29] AghaKouchak A, Huning LS, Mazdiyasni O, Mallakpour I, Chiang F, Sadegh M, et al. How

629 do natural hazards cascade to cause disasters? Nature 2018;561:458–60. doi:10.1038/d41586-

630 018-06783-6.

631 [30] Gill JC, Malamud BD. Reviewing and visualizing the interactions of natural hazards. Rev

632 Geophys 2014;52:680–722. doi:10.1002/2013RG000445.

633 [31] Kappes MS, Keiler M, von Elverfeldt K, Glade T. Challenges of analyzing multi-hazard risk:

634 a review. Nat Hazards 2012;64:1925–58. doi:10.1007/s11069-012-0294-2.

635 [32] Terzi S, Torresan S, Schneiderbauer S, Critto A, Zebisch M, Marcomini A. Multi-risk

636 assessment in mountain regions: A review of modelling approaches for climate change

637   adaptation. J Environ Manage 2019;232:759–71.

638   doi:https://doi.org/10.1016/j.jenvman.2018.11.100.

639   [33]   Forzieri G, Feyen L, Russo S, Vousdoukas M, Alfieri L, Outten S, et al. Multi-hazard

640   assessment in Europe under climate change. Clim Change 2016;137:105–19.

641   doi:10.1007/s10584-016-1661-x.

642   [34]   Gallina V, Torresan S, Critto A, Sperotto A, Glade T, Marcomini A. A review of multi-risk

643   methodologies for natural hazards: Consequences and challenges for a climate change impact

644   assessment. J Environ Manage 2016;168:123–32.

645   doi:http://dx.doi.org/10.1016/j.jenvman.2015.11.011.

646   [35]   UNISDR. Sendai Framework for Disaster Risk Reduction 2015 - 2030. Third World Conf

647   Disaster Risk Reduction, Sendai, Japan, 14-18 March 2015 2015:1–25.

648   doi:A/CONF.224/CRP.1.

649   [36]   Kargel JS, Leonard GJ, Shugar DH, Haritashya UK, Bevington A, Fielding EJ, et al.

650   Geomorphic and geologic controls of geohazards induced by Nepal's 2015 Gorkha

651   earthquake. Science (80-) 2016;351:aac8353. doi:10.1126/science.aac8353.

652   [37]   De Luca P, Hillier JK, Wilby RL, Quinn NW, Harrigan S. Extreme multi-basin flooding

653   linked with extra-tropical cyclones. Environ Res Lett 2017;12:114009.

654   [38]   Ward PJ, Couasnon A, Eilander D, Haigh ID, Hendry A, Muis S, et al. Dependence between

655   high sea-level and high river discharge increases flood hazard in global deltas and estuaries.

656   Environ Res Lett 2018;13:84012. doi:10.1088/1748-9326/aad400.

657   [39]   Collet L, Harrigan S, Prudhomme C, Formetta G, Beevers L. Future hot-spots for hydro-

658   hazards in Great Britain: a probabilistic assessment. Hydrol Earth Syst Sci 2018;22:5387–401.

659   doi:10.5194/hess-22-5387-2018.

660   [40]   Wilby RL, Jones PD, Lister DH. Decadal variations in the nocturnal heat island of London.

661   Weather 2011;66:59–64. doi:10.1002/wea.679.

662   [41]   Merz B, Aerts J, Arnbjerg-Nielsen K, Baldi M, Becker A, Bichet A, et al. Floods and climate:

663   emerging perspectives for flood risk assessment and management. Nat Hazards Earth Syst Sci

664   2014;14:1921–42. doi:10.5194/nhess-14-1921-2014.

665   [42]   Conticello F, Cioffi F, Merz B, Lall U. An event synchronization method to link heavy rainfall

666   events and large-scale atmospheric circulation features. Int J Climatol 2018;38:1421–37.

667   doi:10.1002/joc.5255.

668   [43]   Farnham DJ, Doss-Gollin J, Lall U. Regional Extreme Precipitation Events: Robust Inference

669   From Credibly Simulated GCM Variables. Water Resour Res 2018;54:3809–24.

670   doi:10.1002/2017WR021318.

671   [44]   Murawski A, Vorogushyn S, Bürger G, Gerlitz L, Merz B. Do Changing Weather Types

672   Explain Observed Climatic Trends in the Rhine Basin? An Analysis of Within- and Between-

673   Type Changes. J Geophys Res Atmos 2018;123:1562–84. doi:10.1002/2017JD026654.

674   [45]   Pattison I, Lane SN. The relationship between Lamb weather types and long-term changes in

675   flood frequency, River Eden, UK. Int J Climatol 2012;32:1971–89. doi:10.1002/joc.2415.

676   [46]   Matthews T, Murphy C, Wilby RL, Harrigan S. A cyclone climatology of the British-Irish

677   Isles 1871–2012. Int J Climatol 2016;36:1299–312. doi:10.1002/joc.4425.

678   [47]   Wilby RL, Wigley TML. Downscaling general circulation model output: a review of methods

679   and limitations. Prog Phys Geogr Earth Environ 1997;21:530–48.

680   doi:10.1177/030913339702100403.

681   [48]   Xu H, Corte-Real J, Qian B. Developing daily precipitation scenarios for climate change

682   impact studies in the Guadiana and the Tejo basins. Hydrol Earth Syst Sci 2007;11:1161–73.

683   doi:10.5194/hess-11-1161-2007.

684   [49]   Otero N, Sillmann J, Butler T. Assessment of an extended version of the Jenkinson–Collison

685   classification on CMIP5 models over Europe. Clim Dyn 2018;50:1559–79.

686   doi:10.1007/s00382-017-3705-y.

687   [50]   Stryhal J, Huth R. Trends in winter circulation over the British Isles and central Europe in

688   twenty-first century projections by 25 CMIP5 GCMs. Clim Dyn 2018;0:0.

689   doi:10.1007/s00382-018-4178-3.

690   [51]   Woollings T, Barriopedro D, Methven J, Son S-W, Martius O, Harvey B, et al. Blocking and

691   its Response to Climate Change. Curr Clim Chang Reports 2018. doi:10.1007/s40641-018-

692   0108-z.

693   [52]   Taylor KE, Stouffer RJ, Meehl GA. An Overview of CMIP5 and the Experiment Design. Bull

694   Am Meteorol Soc 2011;93:485–98. doi:10.1175/BAMS-D-11-00094.1.

695   [53]   Lamb HH. British Isles Weather types and a register of daily sequence of circulation patterns,

696   1861-1971. Geophysical Memoir 116, London, HMSO; 1972.

697   [54]   Jones PD, Hulme M, Briffa KR. A comparison of Lamb circulation types with an objective

698   classification scheme. Int J Climatol 1993;13:655–63. doi:10.1002/joc.3370130606.

699   [55]   Jones PD, Harpham C, Briffa KR. Lamb weather types derived from reanalysis products. Int J

700   Climatol 2013;33:1129–39. doi:10.1002/joc.3498.

701   [56]   Jenkinson AF, Collison FP. An Initial Climatology of Gales over the North Sea. Synoptic

702   Climatology Branch Memorandum No. 62, Meteorological Office, Bracknell; 1977.

703   [57]   Compo GP, Whitaker JS, Sardeshmukh PD, Matsui N, Allan RJ, Yin X, et al. The Twentieth

704   Century Reanalysis Project. Q J R Meteorol Soc 2011;137:1–28. doi:10.1002/qj.776.

705   [58]   Kalnay E, Kanamitsu M, Kistler R, Collins W, Deaven D, Gandin L, et al. The NCEP/NCAR

706   40-Year Reanalysis Project. Bull Am Meteorol Soc 1996;77:437–71. doi:10.1175/1520-

707   0477(1996)077<0437:TNYRP>2.0.CO;2.

708   [59]   Hulme M, Barrow E. Climate of the British Isles: present, past and future. London: Routledge;

709   1997.

710   [60]   Lamb HH. Types and spells of weather around the year in the British Isles : Annual trends,

711   seasonal structure of the year, singularities. Q J R Meteorol Soc 1950;76:393–429.

712   doi:10.1002/qj.49707633005.

713 [61] Hulme M, Briffa KR, Jones PD, Senior CA. Validation of GCM control simulations using

714   indices of daily airflow types over the British Isles. Clim Dyn 1993;9:95–105.

715   doi:10.1007/BF00210012.

716 [62] Jones PD, Osborn TJ, Harpham C, Briffa KR. The development of Lamb weather types: from

717   subjective analysis of weather charts to objective approaches using reanalyses. Weather

718   2014;69:128–32. doi:10.1002/wea.2255.

719 [63] Wilby RL. Stochastic weather type simulation for regional climate change impact assessment.

720   Water Resour Res 1994;30:3395–403. doi:10.1029/94WR01840.

721 [64] Gagniuc PA. Markov Chains: From Theory to Implementation and Experimentation. USA,

722   NJ: John Wiley & Sons; 2017. doi:10.1002/9781119387596.

723 [65] Spedicato GA. Discrete Time Markov Chains with R. R J 2017;9:84–104.

724 [66] Mann HB, Whitney DR. On a Test of Whether one of Two Random Variables is

725   Stochastically Larger than the Other. Ann Math Stat 1947;18:50–60.

726   doi:10.1214/aoms/1177730491.

727 [67] Hamed KH, Ramachandra Rao A. A modified Mann-Kendall trend test for autocorrelated

728   data. J Hydrol 1998;204:182–96. doi:https://doi.org/10.1016/S0022-1694(97)00125-X.

729 [68] Sen PK. Estimates of the Regression Coefficient Based on Kendall's Tau. J Am Stat Assoc

730   1968;63:1379–89. doi:10.1080/01621459.1968.10480934.

731 [69] Wilby RL, Quinn NW. Reconstructing multi-decadal variations in fluvial flood risk using

732   atmospheric circulation patterns. J Hydrol 2013;487:109–21.

733   doi:10.1016/j.jhydrol.2013.02.038.

734 [70] O'Hare GPP, Wilby RL. A Review of Ozone Pollution in the United Kingdom and Ireland

735   with an Analysis Using Lamb Weather Types. Geogr J 1995;161:1–20. doi:10.2307/3059923.

736 [71] Pope RJ, Savage NH, Chipperfield MP, Arnold SR, Osborn TJ. The influence of synoptic

737 weather regimes on UK air quality: analysis of satellite column NO $_2$. Atmos Sci Lett

738 2014;15:211–7. doi:10.1002/asl2.492.

739 [72] Pope RJ, Butt EW, Chipperfield MP, Doherty RM, Fenech S, Schmidt A, et al. The impact of

740 synoptic weather on UK surface ozone and implications for premature mortality. Environ Res

741 Lett 2016;11. doi:10.1088/1748-9326/11/12/124004.

742 [73] Woollings T, Harvey B, Masato G. Arctic warming, atmospheric blocking and cold European

743 winters in CMIP5 models. Environ Res Lett 2014;9:14002.

744 [74] Burt TP, Howden NJK. North Atlantic Oscillation amplifies orographic precipitation and river

745 flow in upland Britain. Water Resour Res 2013;49:3504–15. doi:10.1002/wrcr.20297.

746 [75] Murphy JM, Sexton DMH, Jenkins GJ, Boorman PM, Booth BBB, Brown CC, et al. UK

747 Climate Projections Science Report: Climate change projections. Exeter: 2009.

748 [76] Wilby RL. Constructing Climate Change Scenarios of Urban Heat Island Intensity and Air

749 Quality. Environ Plan B Plan Des 2008;35:902–19. doi:10.1068/b33066t.

750 [77] Hess P, Brezowsky H. Katalog der Großwetterlagen Europas.Berichte des Deutschen

751 Wetterdienstes in der US-Zone 33. DeutscherWetterdienst in d. US-Zone: Bad Kissingen.;

752 1952.

753 [78] Prein AF, Bukovsky MS, Mearns LO, Bruyère CL, Done JM. Simulating North American

754 Weather Types With Regional Climate Models. Front Environ Sci 2019;7:36.

755 [79] Kalkstein LS, Nichols MC, Barthel CD, Greene JS. A new spatial synoptic classification:

756 application to air-mass analysis. Int J Climatol 1996;16:983–1004. doi:10.1002/(SICI)1097-

757 0088(199609)16:9<983::AID-JOC61>3.0.CO;2-N.

758

759

760